

MODELING THE SPONTANEOUS CURVATURE EFFECTS IN STATIC CELL MEMBRANE DEFORMATIONS BY A PHASE FIELD FORMULATION

Q. DU, C. LIU, R. RYHAM AND X. WANG

Department of Mathematics
Pennsylvania State University, University Park, PA 16802

ABSTRACT. In this paper, we study the effects of the spontaneous curvature on the static deformation of a vesicle membrane under the elastic bending energy, with prescribed bulk volume and surface area. Generalizing the phase field models developed in our previous works, we deduce a new energy formula involving the spontaneous curvature effects. Several axis-symmetric configurations are obtained through numerical simulations. Some analysis on the effects of the spontaneous curvature on the vesicle membrane shapes are also provided.

1. Introduction. This paper is one in a series of studies on the shape transformation of cell vesicles, using a phase field approach. The goals of such studies are to model, analyze and simulate the deformation and interaction of vesicles with various membrane elastic energies, under different external fields, such as the flow fields or electric fields. More recently, we have successfully developed and applied a phase field model for computing the equilibrium configurations of vesicle membranes that minimize the bending elastic energy [11]. In this paper, the same method is extended to include the effects of spontaneous curvature on a cell membrane.

The usual single component vesicles consists of bilayers assembled by certain amphiphilic molecules in water. They are the simplest models for the biological cells and molecules. The equilibrium shape of such a membrane may be determined by the shape energy. In the isotropic case, it usually consists of the following bending energy [7, 8]:

$$E_{\text{elastic}} = \int_{\Gamma} \frac{k}{2} H^2 ds, \quad (1.1)$$

where $H = (c_1 + c_2)/2$ is the mean curvature of the membrane surface, with c_1 and c_2 as the principle curvatures which are the eigenvalues of the Weingarten matrix of the surface [4]. The parameter k is the bending rigidity, which can depend on the local heterogeneous concentration of the species (such as the protein molecules embedded in the cell membrane). The bending energy given above is a special case of a general form obtained from the Hooke's Law [16, 20, 21, 22, 23]:

$$E = \int_{\Gamma} (a_1 + a_2(H - c_0)^2 + a_3K) ds, \quad (1.2)$$

2000 *Mathematics Subject Classification.* 49Q10, 92B05, 74K15.

Key words and phrases. Phase field, elastic bending energy, cell membrane, spontaneous curvature, numerical simulation, solution branches.

where a_1 is the surface tension, a_2 the bending rigidity and a_3 the stretching rigidity. c_0 is the spontaneous curvature that describes the asymmetry effect of the membrane or its environment. K is the Gaussian curvature. With a constant coefficient a_1 , the first term can be neglected as it remains constant for vesicles with a given surface area. For a smooth compact surface with a constant a_3 , the last term is related to the Euler index which represents the topological structure of the membrane. Such a form has been formulated and studied in the phase field context [12]. For simplicity, here we choose to consider only the energy given in (1.1) and the case where the bending rigidity k is a constant. We note that the asymmetry effect of the lipid bilayer may be attributed to both the intrinsic spontaneous curvature effect of a monolayer, the area difference of a bilayer or even the presence of the protein molecules within the lipid bilayer [2, 9, 10, 16, 17, 18, 19, 22, 23].

If $a_1 = a_3 = 0$ and $a_2 = 1$ in (1.2), the bending energy can be simplified as

$$E = \int_{\Gamma} (H - c_0)^2 ds, \quad (1.3)$$

in which only the effect of the spontaneous curvature is retained and the bending rigidity is assumed to be a constant. The problem considered in this paper is to study the vesicle shapes minimizing the bending energy (1.3) with constraints on the cell volume and surface area. The case for $c_0 = 0$ has been analyzed in [11, 13]. The consideration on the non-zero c_0 case here allows us to make further investigation on the membrane asymmetry effect through numerical simulations. For other related numerical simulations, one may consult [3, 22, 24]. Here, we are able to develop the desired phase field model, to perform numerical simulations, to compute interesting membrane shapes and to analyze the spontaneous effects on the membrane deformation.

The rest of the paper is organized as follows: in section 2, we present the phase field model to include the effect of the spontaneous curvature along with some brief justifications. In section 3, the simulation results with a constant spontaneous curvature are given, and the effect of a non-constant spontaneous curvature is discussed in section 4. Some concluding remarks are made in section 5.

2. Phase Field Model Incorporating the Spontaneous Curvature Effect.

Phase field methods describe problems of geometric configuration and deformation in the reference coordinates (from an observer's point of view). The methods have been proven to be successful and efficient in many applications [1, 5, 6, 14, 15]. However, most problems with energy functionals involving complicated curvature terms remain wide open. Here we are concerned with two important issues: the phase field formulation of the original geometric problem and the rigorous mathematical justification of the formulation.

In this section, we first give the phase field formulation to the spontaneous curvature problem, similar to that in [11] which does not address the spontaneous curvature effect. Then we give a formal verification to the convergence of the phase field formulation as the transition thickness approaches zero, since the phase field method can be viewed as a diffusive interface regularization to the original sharp interface problem.

Given a domain Ω in \mathbf{R}^3 , and a smooth compact surface $\Gamma \subset \Omega$ which is the candidate surface that minimizes the bending elastic energy (1.1) under consideration. Let us take a phase field function $\varphi(x) = q\left(\frac{d(x)}{\sqrt{2}\epsilon}\right) = \tanh\left(\frac{d(x)}{\sqrt{2}\epsilon}\right)$ defined for

all $x \in \Omega$, where $d(x)$ is the signed distance between a point x and Γ , positive inside and negative outside; ϵ is a *transition* parameter that is taken to be very small. Such a function φ is used to mark the vesicle membrane through its sharp transition layer. This layer, roughly of thickness on the order of ϵ , gives a diffusive interface description of the membrane (determined as the zero level set of φ).

Following [11], we have $\nabla\varphi = \frac{1}{\sqrt{2\epsilon}}q'\nabla d$, $\nabla_{ij}^2\varphi = \frac{1}{2\epsilon^2}q''\nabla_i d\nabla_j d + \frac{1}{\sqrt{2\epsilon}}q'\nabla^2 d$, $q'(x) = 1 - q^2(x)$ and $q''(x) = -2q(x)(1 - q^2(x))$. Then, we have

$$\begin{aligned} \nabla_{ij}^2 d &= \frac{\sqrt{2\epsilon}\nabla_{ij}^2\varphi}{q'} - \frac{q''}{\sqrt{2\epsilon}q'}\nabla_i d\nabla_j d = \sqrt{2\epsilon}\frac{\nabla_{ij}^2\varphi}{q'} + \sqrt{2\epsilon}\frac{2q}{(1 - q^2)^2}\nabla_i\varphi\nabla_j\varphi \\ &= \frac{\sqrt{2\epsilon}}{1 - q^2}(\nabla_{ij}^2\varphi + \frac{2q}{1 - q^2}\nabla_i\varphi\nabla_j\varphi) = \frac{\sqrt{2\epsilon}}{1 - \varphi^2}(\nabla_{ij}^2\varphi + \frac{2\varphi}{1 - \varphi^2}\nabla_i\varphi\nabla_j\varphi). \end{aligned}$$

Since $|\nabla\varphi|^2 = \frac{1}{2\epsilon^2}(1 - \varphi^2)^2$, we have an expression for the mean curvature:

$$\begin{aligned} H &= -\frac{1}{2}tr(\nabla^2 d) = -\frac{\sqrt{2\epsilon}}{2(1 - \varphi^2)}(\Delta\varphi + \frac{2\varphi}{1 - \varphi^2}|\nabla\varphi|^2) \\ &= -\frac{\sqrt{2\epsilon}}{2(1 - \varphi^2)}(\Delta\varphi + \frac{1}{\epsilon^2}\varphi(1 - \varphi^2)). \end{aligned}$$

In addition, $\int_{-\infty}^{+\infty}(1 - q^2(\frac{x}{\sqrt{2\epsilon}}))^2 dx = \frac{4\sqrt{2\epsilon}}{3}$, so the bending energy is defined by

$$\begin{aligned} W(\varphi) &= \int_{\Gamma} k(H - c_0)^2 ds \\ &= \frac{3}{4\sqrt{2\epsilon}}\int_{-\infty}^{+\infty}(1 - q^2(\frac{\tau}{\sqrt{2\epsilon}}))^2 d\tau \int_{\Gamma} k(H - c_0)^2 ds \\ &\sim \frac{3}{4\sqrt{2\epsilon}}\int_{\Omega}(1 - \varphi^2(x))^2 k\left(\frac{\epsilon}{\sqrt{2}(1 - \varphi^2)}(\Delta\varphi + \frac{1}{\epsilon^2}\varphi(1 - \varphi^2)) + c_0\right)^2 dx \\ &= \frac{3k}{8\sqrt{2\epsilon}}\int_{\Omega}\left(\epsilon\Delta\varphi + (\frac{1}{\epsilon}\varphi + c_0\sqrt{2})(1 - \varphi^2)\right)^2 dx. \end{aligned}$$

To simplify notation, we set $C = \sqrt{2}c_0$ and define the bending energy as

$$E(\varphi) = \int_{\Omega} \frac{1}{\epsilon} \left(\epsilon\Delta\varphi + (\frac{1}{\epsilon}\varphi + C)(1 - \varphi^2) \right)^2 dx. \tag{2.1}$$

Taking $C = 0$ in the above, we recover the bending energy derived in [11]. Moreover, as in [11], we can deduce that

$$A(\varphi) = \int_{\Omega} \frac{1}{2}(\varphi(x) + 1) dx \tag{2.2}$$

approaches to the interior volume of Γ and

$$B(\varphi) = \int_{\Omega} \left(\epsilon|\nabla\varphi|^2 + \frac{1}{2\epsilon}(\varphi^2 - 1)^2 \right) dx \tag{2.3}$$

approaches to $4\sqrt{2}\text{area}(\Gamma)/3$, or about 1.8856 times the area of Γ .

Thus, the generalized phase field model incorporating the spontaneous effect corresponds to the minimization of the bending energy $E(\varphi)$ under the constraints that $A(\varphi)$ and $B(\varphi)$ are constants. The phase field model, as elaborated in [11], has many advantages in the study of vesicle transformations over the sharp interface

models. It has been a popular approach in the study of many free interface problems. Related studies can be found, for example, in [1, 5, 6, 14, 15].

We note that the energy functional is derived for phase field functions of the special form $\tanh\left(\frac{d(x)}{\sqrt{2\epsilon}}\right)$, while the minimization problem is over a much bigger function class. Thus, to check for the consistency, let us now verify that in our model, the minimizer $\varphi(x)$ is approaching $\tanh\left(\frac{d(x)}{\sqrt{2\epsilon}}\right)$ for small ϵ at least in a more general ansatz. The verification remains largely formal and does not constitute a rigorous proof, though it sheds light on the possible analytical justification of the phase field formulation.

With Γ being compact and smooth, for sufficiently small ϵ , we may first construct a feasible solution u_ϵ and a uniform constant M satisfying $A(u_\epsilon) = \alpha, B(u_\epsilon) = \beta$ and $E(u_\epsilon) < M$, similar to the discussion in [13] which leads to the existence of minimizers for the energetic phase field model.

Then we formally take the ansatz $\varphi(x) = q\left(\frac{d(x)}{\epsilon}\right) + \epsilon h(x)$ with q being a smooth function independent of ϵ with $q(\pm\infty) = \pm 1$ and $q'(\pm\infty) = 0$, and h being a compactly supported smooth function, independent of ϵ . Substituting it into $E(\varphi)$ and examining the higher order terms in $\frac{1}{\epsilon}$ first, we have

$$M > E(\varphi) = \int_{\Omega} \frac{1}{\epsilon^3} (q'' - q(q^2 - 1))^2 dx + \int_{\Omega} \frac{1}{\epsilon^2} \Delta d q' (q'' - q(q^2 - 1)) dx + O\left(\frac{1}{\epsilon}\right).$$

Note that in the second term, $q'(q'' - q(q^2 - 1)) = \left(\frac{1}{2}q'^2 - \frac{1}{4}(q^2 - 1)^2\right)'$. Integrating against Δd and applying the boundary conditions on q , we find that the second term is on the order of $O\left(\frac{1}{\epsilon}\right)$. We thus concentrate on the first term. Suppose that $(q''(t^*) - q(t^*)(q^2(t^*) - 1))^2 > \eta$ for some constant η and some $t^* \in \mathbf{R}$. By continuity, there exists a δ such that $(q''(t) - q(t)(q^2(t) - 1))^2 > \eta$ for $t \in (t^* - \delta, t^* + \delta)$. Let $U_{\epsilon,\delta} = \{x \mid d(x)/\epsilon \in (t^* - \delta, t^* + \delta)\}$. Note that $|U_{\epsilon,\delta}| > \tilde{C}\epsilon$ for some constant \tilde{C} depending on Γ . Then

$$M > \frac{1}{\epsilon^2} \tilde{C}\eta + O\left(\frac{1}{\epsilon}\right)$$

for arbitrarily small ϵ . This is a contradiction as M is a uniform constant. Thus, we arrive at $q'' - q(q^2 - 1) = 0$. Together with the boundary condition, we obtain that $q(\cdot)$ is the function $\tanh\left(\frac{\cdot}{\sqrt{2}}\right)$, the form used to derive the energy functional (2.1).

We may further examine the next order terms in the energy expansion:

$$\int_{\Omega} \left(\frac{1}{\epsilon} (q')^2 (\Delta d + 2c_0)^2 - \frac{2}{\epsilon} q' (\Delta d + 2c_0) (3q^2 - 1) h + \frac{1}{\epsilon} (3q^2 - 1)^2 h^2 \right) dx$$

As developed above, the first term converges to $\frac{4\sqrt{2}}{3}$ times the spontaneous curvature energy, $\int_{\Gamma} (H - c_0)^2 dS$. Note in the second term that $(q(q^2 - 1))' = (3q^2 - 1)q'$. Hence an integration may be performed against $(\Delta d + 2c_0)h$ normal to the interface, implying that the second term is bounded as $\epsilon \rightarrow 0$. The third term consequently must satisfy

$$\lim_{\epsilon \rightarrow 0} \frac{1}{\epsilon} \int_{\Omega} (3q^2 - 1)^2 h^2 dx = \lim_{\epsilon \rightarrow 0} \frac{1}{\epsilon} \int_{\Omega} 2h^2 dx < \infty.$$

Since h is independent of ϵ , it follows that $h \equiv 0$. Consequently, we get that the energy functional in the phase field formulation (2.1) converges to the original energy functional (1.3) as $\epsilon \rightarrow 0$.

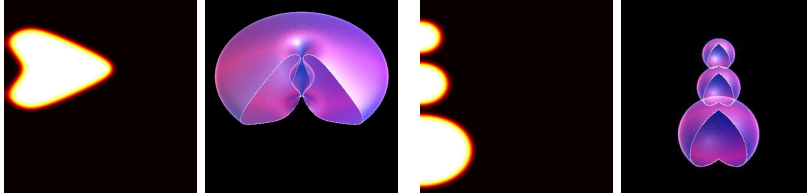


FIGURE 1. Visual illustrations of the cross-section views and full 3-d views of two vesicle shapes.

Further analysis concerning the convergence properties may be provided along the same lines as those presented in [13]. Though a complete theory is yet not available, the formal verification above does provide good indications to the validity and consistency of our phase field model. We next consider the numerical simulations which further substantiate the effectiveness of the model.

To solve the optimization problem in the phase field formulation, we use similar numerical techniques as those developed in [11]. A penalty formulation with penalty coefficients M_1 and M_2 is employed to incorporate the constraints $A(x) = \alpha$ and $B(x) = \beta$. Thus, we are minimizing the functional

$$F(\varphi) = E(\varphi) + M_1 (A(\varphi) - \alpha)^2 + M_2 (B(\varphi) - \beta)^2.$$

The nonlinear variational problem given by the minimization of F is solved via a standard gradient flow approach. The penalty constants are increased until the solution becomes insensitive to the increasing changes in M_1 and M_2 .

We note that a major advantage of the phase field formulation is that one does not need to explicitly track the free surface Γ . For different values of α and β , different surfaces may be obtained, which may involve topological changes and thus presenting numerical difficulties as pointed out in [3]. On the other hand, efficient numerical techniques within the phase field models for detecting the topological change have recently been given in [12]. In the next section, we present examples by implementing the developed techniques. For illustration, in subsequent numerical simulations, we focus on the three dimensional axis-symmetric case only to reduce the computational efforts involved. The full three dimensional simulations are to be reported elsewhere.

3. Surfaces Corresponding to Constant Spontaneous Curvatures. As only axis-symmetric shapes are under considerations, except noted otherwise, most of the vesicles of our numerical experiments are shown by their cross-sections in the r - z plane. The 3-d vesicles are obtained by rotating these two dimensional shapes around the z -axis. To create a three dimensional impression, figure 1 shows the cross-section views and the 3-d cutting views of two vesicle shapes obtained in the later examples. A 45° cut is made in all 3-d views to reveal the interior of the vesicle.

Numerical convergence studies have been performed to assure the validity of the solutions. Indeed, the numerical results presented in this section correspond to simulations using different computational grids. Such different choices are explicitly stated for each simulation as the differences are necessary for maintaining the accuracy of the simulations. We also studied the effect of the parameter ϵ , and we

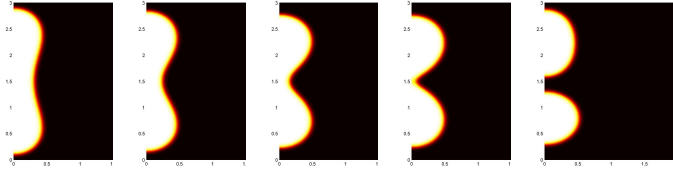


FIGURE 2. Deformation of a gourd with different spontaneous curvatures. $C = 0.0, 1.6, 2.0, 3.0, 4.0$ from left to right.

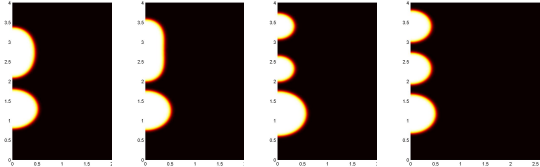


FIGURE 3. Deformation from the last shape of Figure 2 by increasing the surface area ($\beta = 12.00, 12.40, 12.60, 13.40$ from left to right) with the same $C = 4.0$.

only present results for values of ϵ that appear to truthfully characterize the sharp interface limits.

Figure 2 shows the deformation of a gourd shape corresponding to different values of the spontaneous curvature: $C = 0.0, 1.6, 2.0$ and 3.0 (C is in fact $\sqrt{2}$ times of the spontaneous curvature c_0 by our scaling). The grid used for producing this figure is a 150×100 grid where we use a mesh size $h = 0.02$ and $\epsilon = 0.03$. The two constants $\alpha = 1.10$ and $\beta = 12.00$ are fixed for these shapes. We note similar solution branches produced in [3] do not allow the topological changes where the numerical experiments stopped prematurely when a thin neck forms between two components. With the phase field formulation, we are able to handle the topological events smoothly.

A close examination of the shapes in figure 2 leads to the conclusion that a larger value of spontaneous curvature tends to make the vesicle take on the shape of surfaces with constant mean curvatures such as spheres. As a single constant mean curvature surface is not always compatible with the volume and surface constraints, topological transformations thus take place and the gourd finally splits into several smaller spheres for large enough values of the spontaneous curvature. In the last picture of figure 2, one of the two bubbles is in fact almost a perfect sphere. In the next section, there are more examples for the nucleation of these kinds of smaller spheres of different radii if the spontaneous curvature is not a constant.

To further illustrate the spontaneous curvature effect, Figure 3 shows the deformation of the final shape in Figure 2 where the spontaneous curvature and the volume are fixed while the surface area is varying. With the surface area increasing, the ellipsoid splits into two small spheres which eventually grow up to about the same size as the old sphere. The grid for this figure is changed to 200×50 ($h = 0.02$), while other parameters are kept the same: $\epsilon = 0.03$, $\alpha = 1.10$.

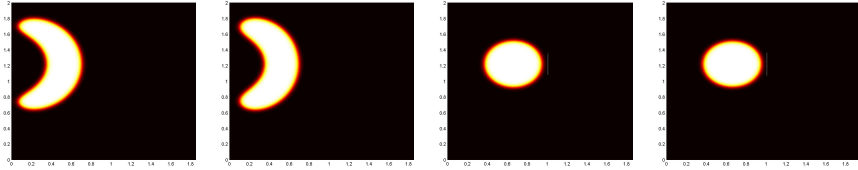


FIGURE 4. Deformation from a bangle to a torus with different spontaneous curvatures. $C = 0.0, 0.4, 0.8$ and 2.8 from left to right.

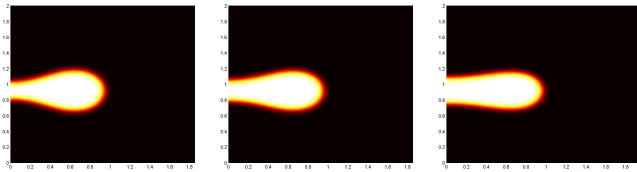


FIGURE 5. Deformation of a dimpled-disk with different spontaneous curvatures. $C = 0.0, 2.0, 8.0$ from left to right.

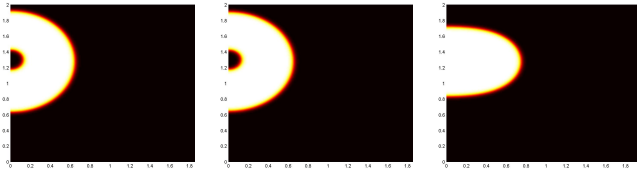


FIGURE 6. Deformation from a longan to an ellipsoid with different spontaneous curvatures. $C = 0.0, 1.0, 2.0$ from left to right.

Figure 4 shows the deformation of a bangle with different spontaneous curvature effect. The grid used in this figure is 200×100 with $h = 0.01$ while other parameters are chosen as $\epsilon = 0.02$, $\alpha = 1.10$ and $\beta = 14.00$. When C changes from 0.0 to 0.4, there is only a minor change taking place to make the shape more sphere like. And when C changes from 0.4 to 0.8, there is a more dramatic deformation and the shape changes from a bangle to a torus. After that, when C increases from 0.8 to 2.8, no obvious change of the shape seems to occur. The simulation result indicates that the torus is a very stable shape for large spontaneous curvatures. Besides the torus, in our experiments, the sphere and the ellipsoid are also very stable for large values of the spontaneous curvature.

Figure 5 shows the deformation of a dimpled-disk with different spontaneous curvatures. Again, the grid used for this figure is 100×100 with $h = 0.02$, while other parameters are given by $\epsilon = 0.03$, $\alpha = 1.10$ and $\beta = 13.00$. When C changes from 0.0 to 2.0, and then later to 8.0, the dimples start to swell.

Figure 6 shows another example of the topological changes of the surface. This corresponds to a deformation from a longan to an ellipsoid with different spontaneous curvatures. The grid used in this figure is 200×100 with $h = 0.01$, $\epsilon = 0.02$,

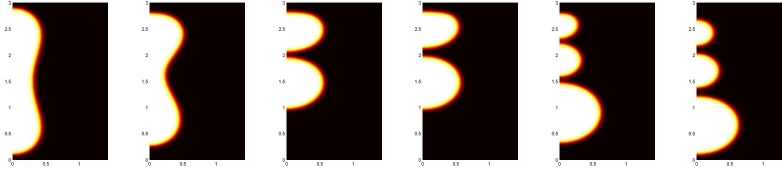


FIGURE 7. Deformation from a gourd to several ellipsoids for non-constant spontaneous curvatures of the form (4.1) with $\sigma = 0.0, 0.2, 0.4, 0.6, 0.8$ and 1.0 , from left to right.

$\alpha = 1.10$ and $\beta = 10.00$. For C in between 0.0 and 1.0 , there is no obvious change, but when C goes from 1.0 to 2.0 , the smaller sphere vanishes.

4. Non-constant Spontaneous Curvature Cases. In the energy formula (2.1), we can allow the spontaneous curvature to vary in space to model the spatial inhomogeneity. We limit our consideration to the case where the spontaneous curvature is always bounded in order to make sure that the phase field function goes to a limiting profile (like the tanh function) as $\epsilon \rightarrow 0$. We note that most choices of the non-constant spontaneous curvatures are artificial but they are motivated by practical considerations, experimental results and other theoretical studies. The numerical algorithms used to simulate the non-constant spontaneous curvature cases largely remain the same as the constant spontaneous curvature case but the actual implementation is slightly more involved because the variational form of the energy may change during the solution process.

Our first numerical example is shown in figure 7, where we take the spontaneous curvature as

$$C = \sigma \begin{cases} (1 + 2z) & \text{for } 0 \leq z < 2.8 \\ 1 & \text{for } z \geq 2.8 \end{cases}, \quad (4.1)$$

which only depends on the domain, not the surface itself. The grid for this figure is 150×100 , $h = 0.02$, and other parameters are $\epsilon = 0.03$, $\alpha = 1.10$ and $\beta = 12.00$.

In figure 7, with c increasing, the gourd splits into smaller and smaller spheres. When c is small, the spheres are likely to stay at positions where the spontaneous curvatures are large so that they lead to a smaller energy, as shown from the second to the fifth graphs. As the spontaneous curvature is specified to be linearly increasing in the z variable, to minimize the energy, the top spheres would tend to stay as high as possible. We thus take C to be a constant for $z \geq 2.8$, so that the spheres would not be all crowded near the top of the computational domain. When c is big enough so that the spontaneous curvature is larger than the curvatures of the spheres, the transformation starts to reverse its course as the spheres are likely to stay at the position with a smaller spontaneous curvature, as shown in the final picture in Figure 7.

Figure 8 shows the energy and the Euler number graph of the shapes shown in Figure 7. As discussed in [12], the Euler number can be computed from the phase field model based on the Gauss-Bonnet formula:

$$\int_{\Gamma} K ds = 2\pi\chi$$

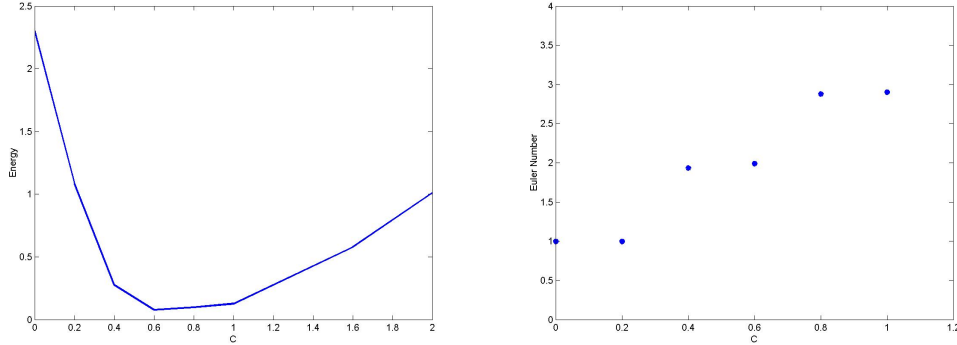


FIGURE 8. The energy (left) and the Euler number (right) graphs of the shapes shown in Figure 7

where the Euler number is $\chi/2$, and K is the Gaussian curvature which may be computed by the phase field function ϕ . Thus, translating into the phase field model, the formula for computing the Euler number for an axis-symmetric shape is given by

$$\frac{\chi}{2} = \iint \frac{\partial_r \phi (\partial_{rr}^2 \phi (\partial_z \phi)^2 + \partial_{zz}^2 \phi (\partial_r \phi)^2 - 2 \partial_r \phi \partial_z \phi \partial_{rz}^2 \phi)}{4((\partial_r \phi)^2 + (\partial_z \phi)^2)^{\frac{3}{2}}} dr dz . \tag{4.2}$$

where the integration is taken on the r - z plan Ω . By taking $\phi = \tanh(\frac{d(x)}{\sqrt{2}\epsilon}) + O(\epsilon^2)$, we can further simplify (4.2) into

$$\frac{\chi}{2} = \frac{35\epsilon}{32\sqrt{2}} \iint \partial_r \phi (1 - \phi^2) ((1 - \phi^2) \Delta \phi + 2\phi |\nabla \phi|^2) dr dz + O(\epsilon) . \tag{4.3}$$

where the operators ∇ and Δ are taken in the r - z plane. We refer to [12] for details of above formulae (4.2) and (4.3).

With the spontaneous curvature increasing, the energy first decreases and then increases with its minimum reached at $c = 0.6$. The right graph shows the Euler number of the shapes, which increase step by step from 1 to 2 then to 3 while the shape splits from one sphere into two and three spheres, which demonstrates the effectiveness of the phase field formulation of the Euler number as a measure to capture topological events.

Note also that the position when the energy reaches its minimum is a critical point. Beyond such a point, the vesicle shape splits into three spheres and the spheres are going to stay at positions with smaller values of the spontaneous curvature.

In general, the spontaneous curvature depends on the vesicle shape itself. Thus, in the next experiment, we consider the case where the spontaneous curvature depends on the direction of the normal vector to the surface. In this case, the energy functional is given by

$$E(\varphi) = \int_{\Omega} \frac{1}{\epsilon} (\epsilon \Delta \varphi + \frac{1}{\epsilon} \varphi (1 - \varphi^2) + C(1 - \varphi^2)(4\epsilon^2 \varphi_z^2 - 1))^2 dx .$$

Since the phase field boundary is measured by $\sqrt{2}\epsilon$, the spontaneous curvature is in fact $c_0 = C(4\epsilon^2 \varphi_z^2 - 1)/\sqrt{2}$, which is $C/\sqrt{2}$ when the normal vector is parallel

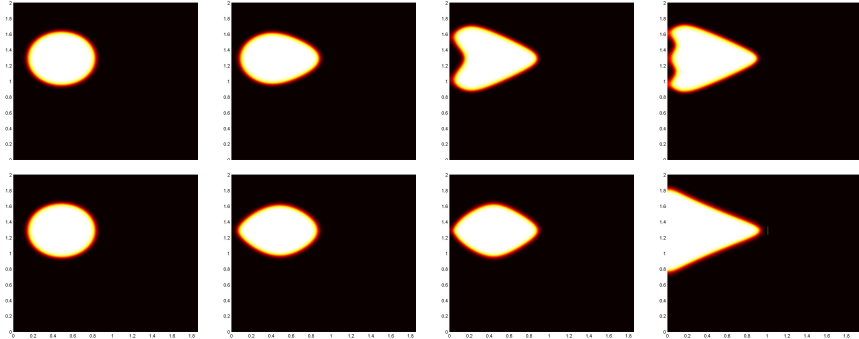


FIGURE 9. Deformation of a torus with non-constant spontaneous curvatures $c_0 = C(4\epsilon^2\varphi_z^2 - 1)/\sqrt{2}$. From left to right, $C = 0, 5, 10, 15$ in the top row, $C = 0, -5, -10, -15$ in the bottom.

to the z-axis, and it changes to $-C/\sqrt{2}$ when the normal vector is perpendicular to the z-axis.

Figure 9 shows the deformation of a torus corresponding to this non-constant spontaneous curvature. The grid for this figure is 200×100 , $h = 0.01$, $\epsilon = 0.02$, $\alpha = 1.10$ and $\beta = 12.00$. Based on results of previous simulations, we know that the torus is very stable with a constant spontaneous curvature. If the spontaneous curvature is non-constant, it may deform into many exotic shapes. In the first row, the spontaneous curvature is positive at both the top and the bottom of the torus while it is negative at the position where the normal vector is perpendicular to the z-axis. In the second row, the spontaneous curvature changes in the reverse direction of the first row. And the resulting behavior is very different, indicating the existence of hysteresis.

Our final experiment shows how the *singular* change in spontaneous curvature affects the vesicle shapes, that is, the spontaneous curvature effect exists only at a point or a tiny part of the surface which often happens when a large molecule sticks onto a bio-membrane. Figure 10 shows the case where C is a non-zero constant only on the surface where the points are close to the axis ($r < 0.1$). The surface bulks gradually when the spontaneous curvature increases at the top and bottom. This experiment suggests why attached viruses cause cells to grow bulges on their surface, that is, this could be from the large spontaneous curvature effects at those bulges. The grid for this figure is 200×100 with $h = 0.01$, and the parameters are $\epsilon = 0.02$, $\alpha = 0.30$ and $\beta = 4.20$.

The experimental investigations on the non-constant spontaneous curvature effects also demonstrate another advantage of our phase field approach to model the cell membrane deformations: it is convenient to incorporate the spatial inhomogeneity into the model.

5. Conclusion. In this paper, we studied the effect of the spontaneous curvature on the static deformation of a vesicle membrane under the elastic bending energy, with prescribed bulk volume and surface area. We deduced the variational phase field formulation incorporating the spontaneous curvature effect. And using this phase field model, we discovered several axial symmetric configurations

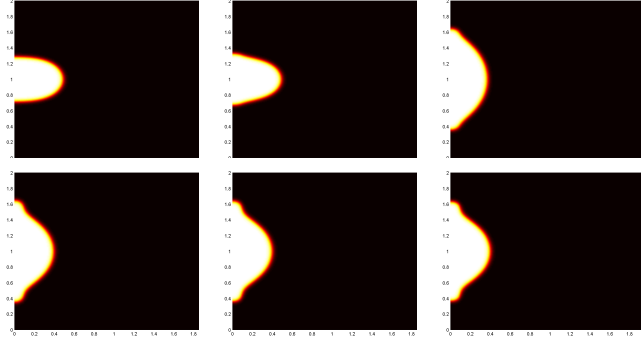


FIGURE 10. From left to right, top to bottom: deformation of an ellipsoid for nonzero spontaneous curvatures $C = 0.0, 5.0, 10.0, 15.0, 20.0$ and 25.0 only in the region $r < 0.1$.

using numerical simulations. We made some analysis on how the constant spontaneous curvature affects the vesicle membrane shapes. Also, some examples of the non-constant spontaneous curvatures were provided. The experiments provide convincing evidence that our phase field approach can effectively incorporate the spontaneous curvature effect and spatial inhomogeneities. Our model can handle topological changes in the deformation of membrane shapes and also capture such events by retrieving useful topological information reliably. We note again that our numerical experiments are constrained to the z-axis symmetric cylindrical geometries. To compare with earlier results concerning non-axisymmetric patterns and those using the area-difference-elasticity (ADE) models as given in [17, 18], more extensive three dimensional simulations will need to be carried out. We will also perform more detailed theoretical and numerical analysis in our future works.

Acknowledgments. The research of Q. Du and X. Wang is supported in part by NSF-DMS 0409297 and NSF-ITR 0205232. The research of C. Liu is supported in part by NSF-DMS 0405850.

References

- [1] D. Anderson, G. McFadden and A. Wheeler, *A diffuse-interface methods in fluid mechanics*, Ann. Rev. Fluid Mech., 30 (1998), 139–165.
- [2] H. Aranda-Espinoza, A. Berman, N. Dan, P. Pincus and S. Safran, *Interaction between inclusions embedded in membranes*, Biophysical Journal, 71 (1996), 648–656.
- [3] M. Bloor and M. Wilson, *Method for efficient shape parameterization of fluid membranes and vesicles*, Phys. Rev. E, 61 (2000), 4218–4229.
- [4] M. Do Carmo, *Differential Geometry of Curves and Surfaces*, Prentice Hall, New Jersey, 1976.
- [5] G. Caginalp and X. F. Chen, *Phase field equations in the singular limit of sharp interface problems*, in “On the evolution of phase boundaries”, Springer, New York, 1992, 1–27.
- [6] Z. Chen and K. Hoffmann, *An error estimate for a finite-element scheme for a phase field model*, IMA J. Numer. Anal., 14 (1994), 243–255.
- [7] P. G. Ciarlet, *Introduction to linear shell theory*, Series in Applied Mathematics (Paris), vol. 1, Gauthier-Villars, Éditions Scientifiques et Médicales Elsevier, Paris, 1998.
- [8] P. G. Ciarlet, *Mathematical elasticity, III*, Studies in Mathematics and its Applications, Vol. 29, North-Holland Publishing Co., Amsterdam, 2000.

- [9] H. Döbereiner, O. Selchow, and R. Lipowsky, *Spontaneous curvature of fluid vesicles induced by trans-bilayer sugar asymmetry*, Eur Biophys J, 28 (1999), 174–178.
- [10] H. Döbereiner, E. Evans, M. Kraus, U. Seifert, and M. Wortis, *Mapping vesicle shapes into the phase diagram: a comparison of experiment and theory*, Phys Rev E, 55 (1997), 4458–4474.
- [11] Q. Du, C. Liu, and X. Wang, *A phase field approach in the numerical study of the elastic bending energy for vesicle membranes*, Journal of Computational Physics, 198 (2004), 450–468.
- [12] Q. Du, C. Liu, and X. Wang, *Retrieving Topological Information For Phase Field Models*, to appear in SIAM Journal on Applied Mathematics (2005).
- [13] Q. Du, C. Liu, R. Ryham and X. Wang, *A Phase Field Formulation of the Willmore Problem*, to appear in J. of Nonlinearity (2005).
- [14] X. Feng and A. Prohl, *Analysis of a fully discrete finite element method for the phase field model and approximation of its sharp interphase limits*, Mathematics of Computation, 73 (2004), 541–567.
- [15] W. George and J. Warren, *A parallel 3d dendritic growth simulator using the phase-field method*, Journal of Computational Physics, 177 (2002), 264–283.
- [16] W. Helfrich, *Elastic properties of lipid bilayers: theory and possible experiments*. Z. Naturforsch. C, 28 (1973), 693–703.
- [17] M. Jaric, U. Seifert, W. Wintz and M. Wortis, *Vesicular instabilities: The prolate-to-oblate transition and other shape instabilities of fluid bilayer membranes*, Phys. Rev. E, 52 (1995), 6623–6634.
- [18] Y. Jie, Q. Liu, J. Liu and Z. Ou-Yang, *Numerical observation of nonaxisymmetric vesicles in fluid membranes*, Phys. Rev. E, 58 (1998), 4730–4736.
- [19] L. Miao, U. Seifert, M. Wortis, and H. Döbereiner, *Budding transitions of fluid-bilayer vesicle: The effect of area-difference elasticity*, Physical Review E, 49 (1994), 5389–5407.
- [20] Z. Ou-Yang, *Anchor Ring-vesicle Membranes*, Physical Review A, 41 (1990), 4517–4520.
- [21] Z. Ou-Yang and W. Helfrich, *Bending energy of vesicle membranes: General expressions for the first, second and third variation of the shape energy and applications to spheres and cylinders*, Physical Review E, 39 (1989), 5280–5288.
- [22] Z. Ou-Yang, J. Liu, and Y. Xie, *Geometric Methods in the Elastic Theory of Membranes in Liquid Crystal Phases*, World Scientific, Singapore, 1999.
- [23] U. Seifert, *Configurations of fluid membranes and Vesicles*, Advances in Physics, 46 (1997), 13–137.
- [24] U. Seifert, K. Berndl and R. Lipowsky, *Configurations of fluid membranes and Vesicles*, Physical Rev A , 44 (1991), 1182–1202.

Received November 2004; revised April 2005.

E-mail address: qdu@math.psu.edu

E-mail address: liu@math.psu.edu

E-mail address: ryham@math.psu.edu

E-mail address: wang@math.psu.edu